Effects of chemical reaction on mixed convection flow of a polar fluid through a porous medium in the presence of internal heat generation

P. M. Patil, Ali J. Chamkha & S. Roy

Meccanica
An International Journal of Theoretical and Applied Mechanics AIMETA

ISSN 0025-6455
Volume 47
Number 2

Meccanica (2012) 47:483-499
DOI 10.1007/s11012-011-9443-z

Springer

Your article is protected by copyright and all rights are held exclusively by Springer Science+Business Media B.V.. This e-offprint is for personal use only and shall not be self-archived in electronic repositories. If you wish to self-archive your work, please use the accepted author's version for posting to your own website or your institution's repository. You may further deposit the accepted author's version on a funder's repository at a funder's request, provided it is not made publicly available until 12 months after publication.

Author's personal copy

Meccanica (2012) 47:483–499
DOI 10.1007/s11012-011-9443-z

Effects of chemical reaction on mixed convection flow of a polar fluid through a porous medium in the presence of internal heat generation

P.M. Patil · Ali J. Chamkha · S. Roy

Received: 30 May 2009 / Accepted: 14 June 2011 / Published online: 1 July 2011
© Springer Science+Business Media B.V. 2011

Abstract This paper reports a detailed numerical investigation on mixed convection flow of a polar fluid through a porous medium due to the combined effects of thermal and mass diffusion. The energy equation accounts for heat generation or absorption, while the *n*th order homogeneous chemical reaction between the fluid and the diffusing species is included in the mass diffusion equation. The governing equations of the linear momentum, angular momentum, energy and concentration are obtained in a non-similar form by introducing a suitable group of transformations. The final set of non-similar coupled non-linear partial differential equations is solved using an implicit finite-difference scheme in combination with quasi-linearization technique. The effects of various parameters on the velocity, angular velocity, temperature and concentration fields are investigated. Numerical results for the skin friction coefficient, wall stress of angular velocity, Nusselt number and Sherwood number are also presented.

Keywords Mixed convection · Polar fluid · Porous medium · Heat generation · Chemical reaction · Quasi-linearization method

P.M. Patil
Department of Mathematics, JSS's Banashankari Arts, Commerce and Shanti Kumar Gubbi Science College, Vidyagiri, Dharwad 580 004, India
e-mail: pmpmath@gmail.com

A.J. Chamkha (✉)
Manufacturing Engineering Department, The Public Authority for Applied Education and Training, Shuweikh 70654, Kuwait
e-mail: achamkha@yahoo.com

S. Roy
Department of Mathematics, I.I.T. Madras, Chennai 600 036, India
e-mail: sjroy@iitm.ac.in

1 Introduction

Convective flows in porous media have been extensively studied during the last several decades. These studies have included several different physical effects. A convection situation, in which effects of both forced and free convection are significant, is commonly referred to as mixed convection or combined convection. The effect is especially pronounced in situations where the forced fluid flow velocity is moderate and/or the temperature difference is very large. In mixed convection flows, the forced convection effects and the free convection effects are of comparable magnitude. Thus, in this situation, both the forced and free convections occur simultaneously, i.e. mixed convection occurs in which the effect of buoyancy forces on a forced flow or the effect of forced flow on buoyant flow is significant. Mixed convection flow through porous media occurs in a variety of technological and industrial applications, as well as in many natural circumstances, such as storage of nuclear waste material,

Author's personal copy

packed-bed reactors, pollutant dispersion in aquifers, geothermal extraction, industrial and agricultural distribution, ground water flows, cooling of electronic components, thermal insulation engineering, food processing, casting and welding of manufacturing processes, the dispersion of chemical contaminants in various processes in the chemical industry and in the environment, soil pollution, fibrous insulation and even for obtaining approximate solutions for flow through turbo-machinery. This topic is of prime importance in all these applications, thereby stimulating the need for a full understanding of transport phenomena in porous media. Comprehensive theories and experiments of thermal convection in porous media and review of literature, with special emphasis on practical applications, have been reported in the recent books by Nield and Bejan [1], Ingham and Pop [2], Vafai [3], Ingham et al. [4] and Bejan et al. [5].

Merkin [6, 7] has studied dual solutions occurring in the problem of the mixed convection flow over a vertical surface through a porous medium with constant temperature for the case of opposing flow. Aly et al. [8] and Nazar and Pop [9] have investigated the existence of dual solutions for mixed convection in porous medium. Chin et al. [10] have investigated the steady mixed convection boundary layer flow over a vertical impermeable surface embedded in a porous medium when the viscosity of the fluid varies inversely as a linear function of the temperature. In this study, both the cases of assisting and opposing flows are considered.

The growing need for chemical reactions in chemical and hydrometallurgical industries requires the study of heat and mass transfer in presence of chemical reaction. There are many transport processes that are governed by the simultaneous action of buoyancy forces due to both thermal and mass diffusion in presence of chemical reaction effect. These processes are observed in nuclear reactor safety and combustion systems, solar collectors as well as chemical and metallurgical engineering. Their other applications include solidification of binary alloys and crystal growth dispersion of dissolved materials or particulate water in flows, drying and dehydration operations in chemical and food processing plants, evaporation at the surface of a water body, distribution of temperature and moisture over agricultural fields and groves of fruit trees, damage of crops due to freezing, energy transfer in a wet cooling tower and flow in a desert cooler, heat and mass transfer occur simultaneously. Chemical reaction can be modeled as either homogeneous or heterogeneous processes. This depends on whether they occur at an interface or a single phase volume reaction. A homogeneous reaction is one that occurs uniformly throughout a given phase. The species generation in a homogeneous reaction is the same as the internal source of heat generation. On the other hand, heterogeneous reaction takes place in a restricted area or within the boundary of a phase. The order of the chemical reaction depends on several factors. One of the simplest chemical reactions is the first order reaction in which the rate of reaction is directly proportional to the species concentration. In many chemical engineering processes, a chemical reaction between a foreign mass and the fluid does occur. These processes take place in numerous industrial applications, such as the polymer production, the manufacturing of ceramics or glassware, the food processing and so on. The study of heat and mass transfer with chemical reaction is of great practical importance to engineers and scientists because of its almost universal occurrence in many branches of science and engineering. Das et al. [11] have studied the effects of mass transfer on the flow started impulsively past an infinite vertical plate in presence of wall heat flux and chemical reaction. Muthucumaraswamy and Ganeshan [12, 13] have studied the impulsive motion of a vertical plate with heat flux/mass flux/suction and diffusion of chemically reactive species. Seddeek [14] has studied the finite element method for the effects of chemical reaction, variable viscosity, thermophoresis, and heat generation/absorption on a boundary layer hydromagnetic flow with heat and mass transfer over a heat surface. Kandasamy et al. [15, 16] have examined the effects of chemical reaction, heat and mass transfer on with or without MHD flow with heat source/suction. Raptis and Perdikis [17] have examined the effects of viscous flow over a non-linearly stretching sheet in the presence of chemical reaction and magnetic field. Very recently, Jalal et al. [18] have investigated analytically on acceleration motion of a vertically falling spherical particle in incompressible Newtonian media. Effects of unsteady rolling motion of spheres in inclined tubes filled with incompressible Newtonian fluids have been studied by Jalal and Ganji [19]. An analytical study on motion of a sphere rolling down an inclined plane submerged in a Newtonian fluid was made by Jalal and Ganji [20]. Jalal et al. [21] have also studied analytically on settling of non-spherical particles.

Author's personal copy

In recent times, interest in problems of non-Newtonian fluids has increased considerably because of more and more applications in chemical process industries, food preservation techniques, petroleum production, power engineering, etc. The non-Newtonian boundary layer flows through porous medium with heat and mass transfer are seen in such wide applications as fluid film lubrication, analysis of polymer in chemical engineering, etc. The fluids which sustain couple stresses, called polar fluids, model those fluids with micro-structures, which are mechanically significant when the characteristic dimension of the problem is of the same order of magnitude as the size of the micro-structure. Extensive reviews of the theory can be found in the review article by Cowin [22]. Since the micro-structure size is the same as the average pore size, it is pertinent to study the flow of polar fluids through a porous medium. The examples of fluids which can be modeled as polar fluids are mud, crude oil, body fluids, lubricants with polymer additives, etc. The effects of couple stresses on the flow through a porous medium are studied by Patil and Hiremath [23]. Hiremath and Patil [24] have examined the effects of free convection on the oscillatory flow of a couple stress fluids through a porous medium. Steady flow of a polar fluid through a porous medium by using Forchheimer's model was discussed by Raptis and Takhar [25]. Analytical solutions for the problem of the flow of a polar fluid past a vertical porous plate in the presence of couple stresses and radiation, where the temperature of the plate is assumed to oscillate about a mean value have been obtained by Ogulu [26]. Patil and Kulkarni [27] have examined the effects of chemical reaction on free convective flow of a polar fluid through a porous medium in the presence of internal heat generation. Gorla [28] has discussed the mixed convection in a micropolar fluid past a vertical surface with uniform heat flux. Patil [29] has studied the effects of free convection on the oscillatory flow of a polar fluid through a porous medium in presence of variable heat flux. Free convective oscillatory flow of a polar fluid through a porous medium in the presence of oscillating suction and temperature was examined by Patil and Kulkarni [30].

The aim of the present study is to investigate the effects of chemical reaction and internal heat generation or absorption on mixed convection flow, with heat and mass transfer, of a polar fluid through a porous medium in the presence of couple stresses and prescribed wall heat and mass fluxes. The flow configuration is modeled as hot vertical plate bounding the porous region filled with water containing soluble and insoluble chemical materials. The system of nonlinear coupled partial differential equations governing the flow has been solved numerically using the method of quasi-linearization and an implicit finite difference scheme [31, 32]. The study reveals that the flow field is considerably influenced by the presence of chemical reaction, heat source/sink and couple stresses.

2 Mathematical formulation

We consider steady, laminar, two-dimensional mixed convection flow of a viscous incompressible polar fluid through a porous medium over a semi-infinite vertical porous plate. The x-axis is taken along the vertical plate and y-axis is normal to it. The velocity, angular velocity, temperature and concentration fields are $(u, v, 0)$, $(0, 0, \omega)$, T and C, respectively. Figure 1 shows the coordinate system and the physical model for the flow configuration. The surface is maintained at a prescribed heat flux q_w as well as a mass flux m_w. A heat source or sink is placed within the flow to allow possible heat generation or absorption effects. The concentration of diffusing species is assumed to be very small in comparison with other chemical species far from the surface C_∞, and is infinitely small. Hence the Soret and Dufour effects are neglected. The chemical reactions are taking place in the flow. All thermophysical properties of the fluid in the flow model are assumed to be constant except the density variations causing the body force term in the momentum equation. The Boussinesq approximation is invoked for the fluid properties to relate density changes, and to couple in this way the temperature and concentration fields, $g[\beta_T(T - T_\infty) + \beta_C(C - C_\infty)]$ to the flow field [33]. Under the above assumptions, the equations of conservation of mass, momentum, angular momentum, energy and concentration governing the problem of mixed convection boundary layer flow along a plate in a porous medium are given by:

$$\frac{\partial u}{\partial x} + \frac{\partial v}{\partial y} = 0, \tag{1}$$

Author's personal copy

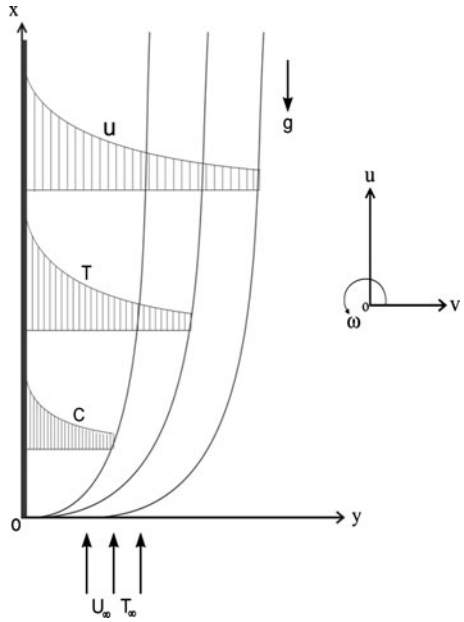

Fig. 1 Flow model and coordinate system

$$u\frac{\partial u}{\partial x}+v\frac{\partial u}{\partial y}=(\nu+\nu_r)\frac{\partial^2 u}{\partial y^2}+2\nu_r\frac{\partial \omega}{\partial y}+g[\beta_T(T-T_\infty)+\beta_C(C-C_\infty)]-\frac{\nu+\nu_r}{K}(u-U_\infty), \tag{2}$$

$$u\frac{\partial \omega}{\partial x}+v\frac{\partial \omega}{\partial y}=\frac{\gamma}{I}\frac{\partial^2 \omega}{\partial y^2}, \tag{3}$$

$$u\frac{\partial T}{\partial x}+v\frac{\partial T}{\partial y}=\frac{\lambda}{\rho C_P}\frac{\partial^2 T}{\partial y^2}\pm\frac{Q_0}{\rho C_P}(T-T_\infty), \tag{4}$$

$$u\frac{\partial C}{\partial x}+v\frac{\partial C}{\partial y}=D\frac{\partial^2 C}{\partial y^2}-k_1(C-C_\infty)^n, \tag{5}$$

where $\gamma=(C_a+C_d)I^{-1}$.

The appropriate boundary conditions are:

$$\begin{aligned} &y=0:\quad u=0,\quad v=0,\quad \frac{\partial \omega}{\partial y}=-m\frac{\partial^2 u}{\partial y^2},\\ &-k\frac{\partial T}{\partial y}=q_w,\quad -D\frac{\partial C}{\partial y}=m_w,\\ &y\to\infty:\quad u\to U_\infty,\quad \omega\to 0,\quad T\to T_\infty,\\ &C\to C_\infty. \end{aligned} \tag{6}$$

The boundary conditions (6) are derived on the basis of the assumption that the couple stresses are dominant during the rotation of the particles. Further, m is a constant and $0\le m\le 1$. The case $m=0$, which corresponds to $\frac{\partial \omega}{\partial y}=0$ at the wall represents concentrated particle flows in which the micro elements close to the wall surface are not able to rotate. This case is known as strong concentration of micro elements. The case $m=0.5$, which corresponds to the vanishing of antisymmetric part of the stress tensor and indicates weak concentration of micro elements. The case $m=1.0$, which corresponds to the modeling of turbulent boundary layer flows. Here, we shall consider the case of $m=0.5$.

If $\psi(x,y)$ represents the stream function, then

$$u=\frac{\partial \psi}{\partial y},\quad v=-\frac{\partial \psi}{\partial x}. \tag{7}$$

Introducing the non-dimensional quantities:

$$\begin{aligned} &\xi=\frac{x}{L},\quad \eta=\left(\frac{U_\infty}{\nu x}\right)^{1/2}y,\\ &\psi(x,y)=(\nu U_\infty x)^{1/2}f(\xi,\eta),\\ &\omega=\left(\frac{U_\infty}{\nu x}\right)^{1/2}U_\infty\Omega(\xi,\eta),\quad u=U_\infty\frac{\partial f}{\partial \eta},\\ &v=-\frac{(\nu U_\infty x)^{1/2}}{2x}(f(\xi,\eta)+2\xi f_\xi-\eta f_\eta),\quad \alpha=\frac{\nu_r}{\nu},\\ &f_\eta(\xi,\eta)=F(\xi,\eta),\quad \beta=\frac{I\nu}{\gamma},\quad \mathrm{Re}_L=\frac{U_\infty L}{\nu},\\ &Da=\frac{K}{L^2},\quad (T-T_\infty)=\left(\frac{q_w}{k}\right)\left(\frac{\nu x}{U_\infty}\right)^{1/2}\Theta(\xi,\eta),\\ &(C-C_\infty)=\left(\frac{m_w}{D}\right)\left(\frac{\nu x}{U_\infty}\right)^{1/2}\Phi(\xi,\eta),\\ &Q=\frac{Q_0 L}{\rho C_p U_\infty},\quad Gr=\frac{g\beta_T q_w L^4}{k\nu^2\mathrm{Re}_L^{1/2}},\\ &Gr^*=\frac{g\beta_C m_w L^4}{D\nu^2\mathrm{Re}_L^{1/2}},\quad \lambda=\frac{Gr}{\mathrm{Re}_L^2},\quad \lambda^*=\frac{Gr^*}{\mathrm{Re}_L^2},\\ &N=\frac{\lambda^*}{\lambda},\quad Pr=\frac{\rho\nu C_p}{k},\\ &\Delta=k_1\left(\frac{m_w}{D}\right)^{n-1}(\mathrm{Re}_L)^{-(\frac{n-1}{2})}\left(\frac{L^n}{U_\infty}\right),\quad Sc=\frac{\nu}{D} \end{aligned} \tag{8}$$

Author's personal copy

into (2)–(5), we obtain the following non-dimensional equations:

$$F_{\eta\eta} + \frac{f}{2(1+\alpha)}F_\eta - \frac{\xi}{Da\mathrm{Re}_L}(F-1) + \frac{2\alpha}{(1+\alpha)}\Omega_\eta \pm \frac{\lambda}{(1+\alpha)}\xi^{3/2}(\Theta + N\Phi) = \frac{\xi}{(1+\alpha)}\left[F F_\xi - f_\xi F_\eta\right], \tag{9}$$

$$\Omega_{\eta\eta} + \beta\frac{f}{2}\Omega_\eta + \frac{\beta}{2}F\Omega = \beta\xi[F\Omega_\xi - f_\xi\Omega_\eta], \tag{10}$$

$$\Theta_{\eta\eta} + \frac{Prf}{2}\Theta_\eta + Pr\left(Q\xi - \frac{1}{2}F\right)\Theta = Pr\xi[F\Theta_\xi - f_\xi\Theta_\eta], \tag{11}$$

$$\Phi_{\eta\eta} + \frac{Scf}{2}\Phi_\eta - \frac{Sc}{2}F\Phi - Sc\Delta\xi^{\frac{n+1}{2}}\Phi^n = Sc\xi\left[F\Phi_\xi - f_\xi\Phi_\eta\right]. \tag{12}$$

Where $f = \int_0^\eta F d\eta + f_w$; $f_w = 0$. Here F is the derivative of f. That is $F = f'$. It should be noted that f_w is taken to be zero since the plate is impermeable. That is there is no suction or injection.

The corresponding boundary conditions (6) reduce to the following non-dimensional form:

$$\begin{aligned} &F = 0, \quad \Omega_\eta = -mF_{\eta\eta}, \quad \Theta_\eta = -1, \quad \Phi_\eta = -1, \\ &\text{at} \quad \eta = 0, \\ &F \to 1, \quad \Omega \to 0, \quad \Theta \to 0, \quad \Phi \to 0 \\ &\text{as} \quad \eta \to \infty. \end{aligned} \tag{13}$$

It is worth mentioning here that $T_w > T_\infty$ refers to a heated plate (assisting flow) and $T_w < T_\infty$ for a cooled plate (opposing flow). Therefore, the mixed convection (buoyancy) parameter appearing in (9) $\lambda > 0$ indicates for assisting flow and $\lambda < 0$ for opposing flow, respectively.

The momentum equation (9) is coupled with all the other equations of the system. The material parameter α appearing in (9) is the non-dimensional parameter representing the ratio between the rotational kinematic viscosity (ν_r) and kinematic viscosity (ν). Another material parameter β appearing in (10) is non-dimensional parameter representing the ratio between the kinematic viscosity and coefficients of couple stress viscosities. Both the material parameters α and β characterize the polarity of the fluid. When $\alpha = 0$ and $\beta = 0$, the problem reduces to the corresponding Newtonian case. The ratio of buoyancy forces N appearing in (9) is the non-dimensional parameter representing the ratio between the buoyancy force due to concentration difference and the buoyancy force due to temperature difference. The parameter N is zero for no buoyancy effect due to mass diffusion, is infinite for no buoyancy effect due to thermal diffusion, is unity for thermal and mass buoyancy forces of the same strength, positive (>0) for the combined buoyancy forces driving the flow and negative (<0) for the buoyancy forces opposing each other. The heat generation or absorption parameter Q appearing in (11) is the non-dimensional parameter based on the amount of heat generated or absorbed per unit volume given by $Q_0(T - T_\infty)$, Q_0 being constant coefficient, which may take either positive or negative values. The source term represents the heat generation when Q is positive (>0) and the heat absorption when Q is negative (<0). The parameter Q is zero in case of no heat source. The chemical reaction parameter Δ appearing in (12) is the non-dimensional parameter representing the generation or consumption of the diffusing species. Δ is positive (>0) for species generation, is negative (<0) for species consumption and is zero for no chemical reaction.

The quantities of physical interest, namely, the skin friction coefficient, Nusselt number (or wall heat transfer coefficient) and the Sherwood number (or wall mass transfer coefficient) are defined, respectively, as follows:

$$\mathrm{Re}_L^{1/2}C_f = 2(1+\alpha)\xi^{-1/2}F_\eta(\xi,0), \tag{14}$$

$$C_{fm} = \frac{U_\infty^2}{\nu L}\xi^{-1}\Omega_\eta(\xi,0), \tag{15}$$

$$\mathrm{Re}_L^{-1/2}Nu_x = \frac{\xi^{1/2}}{\Theta(\xi,0)}, \tag{16}$$

$$\mathrm{Re}_L^{-1/2}Sh_x = \frac{\xi^{1/2}}{\Phi(\xi,0)}. \tag{17}$$

3 Method of solution

The set of non-dimensional equations (9)–(12) under the boundary conditions (13) for prescribed heat flux

Author's personal copy

as well as mass flux with the initial conditions obtained from the corresponding steady state equations have been solved numerically using an implicit finite difference scheme in combination with the quasilinearization technique [31, 32]. This method has been proven to be adequate for boundary-layer type equations and gives accurate results. An iterative sequence of linear equations is carefully constructed to approximate the nonlinear equations (9)–(12) under the boundary conditions (13) achieving quadratic convergence and monotonicity. Applying the quasilinearization technique, the nonlinear coupled ordinary differential equations (9)–(12) with boundary conditions (13) are replaced by the following sequence of linear ordinary differential equations.

$$F_{\eta\eta}^{(i+1)} + A_1^i F_\eta^{(i+1)} + A_2^i F^{(i+1)} + A_3^i F_\xi^{(i+1)} + A_4^i \Omega_\eta^{(i+1)} + A_5^i \Theta^{(i+1)} + A_6^i \Phi^{(i+1)} = A_7^i, \quad (18)$$

$$\Omega_{\eta\eta}^{(i+1)} + B_1^i \Omega_\eta^{(i+1)} + B_2^i \Omega^{(i+1)} + B_3^i \Omega_\xi^{(i+1)} + B_4^i F^{(i+1)} = B_5^i, \quad (19)$$

$$\Theta_{\eta\eta}^{(i+1)} + C_1^i \Theta_\eta^{(i+1)} + C_2^i \Theta^{(i+1)} + C_3^i \Theta_\xi^{(i+1)} + C_4 F^{(i+1)} = C_5^i, \quad (20)$$

$$\Phi_{\eta\eta}^{(i+1)} + D_1^i \Phi_\eta^{(i+1)} + D_2^i \Phi^{(i+1)} + D_3^i \Phi_\xi^{(i+1)} + D_4^i F^{(i+1)} = D_5^i. \quad (21)$$

The coefficients in (18)–(21) are given by:

$$A_1^i = (1+\alpha)^{-1}\left(\frac{f}{2} + \xi f_\xi\right),$$

$$A_2^i = -\xi[(Da\mathrm{Re})^{-1} + (1+\alpha)^{-1} F_\xi],$$

$$A_3^i = -\xi(1+\alpha)^{-1} F, \quad A_4^i = 2\alpha(1+\alpha)^{-1},$$

$$A_5^i = \lambda(1+\alpha)^{-1}\xi^{3/2}, \quad A_6^i = \lambda N(1+\alpha)^{-1}\xi^{3/2},$$

$$A_7^i = -\xi[(Da\mathrm{Re}_L)^{-1} + (1+\alpha)^{-1} F F_\xi],$$

$$B_1^i = \beta\left(\frac{f}{2} + \xi f_\xi\right), \quad B_2^i = \frac{\beta F}{2}; \quad B_3^i = -\beta\xi F,$$

$$B_4^i = \beta\left(\frac{\Omega}{2} - \xi\Omega_\xi\right), \quad B_5^i = \beta\left(\frac{\Omega}{2} - \xi\Omega_\xi\right)F,$$

$$C_1^i = Pr\left(\frac{f}{2} + \xi f_\xi\right), \quad C_2^i = Pr\left(\xi Q - \frac{F}{2}\right),$$

$$C_3^i = -Pr\xi F, \quad C_4^i = -Pr\left(\frac{\Theta}{2} + \xi\Theta_\xi\right),$$

$$C_5^i = -Pr\left(\frac{\Theta}{2} + \xi\Theta_\xi\right)F, \quad D_1^i = Sc\left(\frac{f}{2} + \xi f_\xi\right),$$

$$D_2^i = -Sc\left(\frac{F}{2} + n\Delta\xi^{(\frac{n+1}{2})}\Phi^{n-1}\right), \quad D_3^i = -Sc\xi F,$$

$$D_4^i = -Sc\left(\frac{\Phi}{2} + \xi\Phi_\xi\right),$$

$$D_5^i = -Sc\left\{(n-1)\Delta\xi^{(\frac{n+1}{2})}\Phi^n + \left(\frac{\Phi}{2} + \xi\Phi_\xi\right)F\right\}.$$

The coefficient functions with iterative index i are known and the functions with iterative index $(i+1)$ are to be determined. The boundary conditions are given by

$$\begin{aligned} &F^{(i+1)} = 0, \quad \Omega_\eta^{(i+1)} = -mF_{\eta\eta}^{(i+1)},\\ &\Theta^{(i+1)} = \Phi^{(i+1)} = -1 \quad \text{at} \quad \eta = 0,\\ &F^{(i+1)} \to 1, \quad \Omega^{(i+1)} \to 0,\\ &\Theta^{(i+1)} = \Phi^{(i+1)} \quad \to \quad 0, \quad \text{as} \quad \eta \to \eta_\infty, \end{aligned} \quad (22)$$

where η_∞ is the edge of the boundary layer.

Since the method is explained by Inouye and Tate [31] and also in a recent paper by Singh et al. [32], its detailed analysis is not presented here for the sake of brevity. In brief, the nonlinear coupled ordinary differential equations were replaced by an iterative sequence of linear equations following quasilinearization technique. The resulting sequences of linear ordinary differential equations were expressed in difference form using central difference scheme in η-direction. In each iteration step, the equations were then reduced to a system of linear algebraic equations with a block tridiagonal structure which is solved by using Varga algorithm [34].

To ensure the convergence of the numerical solution to exact solution, the step size $\Delta\eta$ and the edge of the boundary layer have been optimized and the result presented here are independent of the step size at least up to the fifth decimal place. The step size of $\Delta\eta$ has been taken as 0.02. A convergence criterion based on the relative difference between the current and previous iteration values is employed. When the difference reaches less than 10^{-5}, the solution is assumed to have converged and the iterative process is terminated.

It should be mentioned that a direct comparison with previously published work on special cases of the

Author's personal copy

current problem is not possible due to the use of different transformation groups for the governing equations. However, it is possible to check the accuracy of the numerical method by comparison with a similar problem although with different coefficients. In fact, we have validated the results of the problem discussed by Elbashbeshy and Bazid [35]. But since the problem is somewhat different from our problem, it is felt that it is not appropriate to add this comparison herein.

4 Result and discussion

The numerical computations have been carried out for various values of the parameters

α $(0.5 \leq \alpha \leq 1.5)$, β $(2.0 \leq \beta \leq 12.0)$,

λ $(0 \leq \lambda \leq 100.0)$, N $(-0.23 \leq N \leq 3.0)$,

Sc $(0.22 \leq Sc \leq 2.57)$, Q $(-1.0 \leq Q \leq 1.0)$,

Δ $(0.1 \leq \Delta \leq 1.0)$, Pr $(0.7 \leq Pr \leq 7.0)$,

Da $(1.0 \leq Da \leq 1000000.0)$, n $(0.0 \leq n \leq 3.0)$.

The edge of the boundary layer (η_∞) has been taken between 3.0 and 9.0 depending on the values of the parameters.

The effects of the ratio of buoyancy forces parameter (N) and the Darcy number (Da) on the velocity $F(\xi, \eta)$, angular velocity $\Omega(\xi, \eta)$, temperature $\Theta(\xi, \eta)$ and concentration $\Phi(\xi, \eta)$ profiles are presented in Figs. 2–5.

The velocity profile $F(\xi, \eta)$ and the skin friction coefficient $(\mathrm{Re}_L^{1/2} C_f)$ are displayed in Figs. 2a and 2b, respectively, for different values of the buoyancy ratio parameter (N) and the Darcy number (Da). It should be noted that the positive values of N imply that both buoyancy forces act in the same direction. On the contrary, the negative values of N appear when thermal and concentration buoyancy forces act in opposite direction. It is observed from Fig. 2a that, for buoyancy-induced aiding flow ($N > 0$), the buoyancy forces show significant overshoot in the velocity profiles near the wall. As N increases, the velocity overshoot increases for buoyancy assisting flow ($\lambda > 0$) near the wall. The physical reason is that the buoyancy forces act like a pressure gradient which accelerates/decelerates the fluid within the boundary layer. The effect of N on the velocity profile is significant because the parameter N is explicitly present only in the momentum equation. In fact, the combined effects of an assisting buoyancy force due to thermal and concentration gradients and heat generation act like a favorable pressure gradient which enhances the fluid acceleration. On the other hand, the magnitude of the overshoot decreases in buoyancy-induced opposing flow ($N < 0$). Further, it is observed that the velocity decreases in porous medium as compared to the without porous medium ($Da \to \infty$). The presence of a porous medium increases the resistance to flow resulting in decreases in the flow velocity and increases in both the fluid temperature and solute concentration. Also, this is in accordance with the fact that increasing the permeability of the porous medium reduces the drag force and hence, causes the flow velocity to increase. The effects of N (the ratio of buoyancy forces) and Darcy number (Da) on the skin friction coefficient $(\mathrm{Re}_L^{1/2} C_f)$ when $\lambda = 2.0, n = 1.0, \beta = 2.0, Sc = 0.22, \Delta = 0.5, Pr = 0.7, \mathrm{Re}_L = 5.0, m = 0.5, \alpha = 1.0$ and $Q = 0.5$ are shown in Fig. 2b. The results indicate that the skin friction coefficient $(\mathrm{Re}_L^{1/2} C_f)$ increases with increasing values of N for both negative and positive values monotonously. This is due to the fact that the increase of N enhances the fluid acceleration and hence, the skin friction coefficient increases. In particular, for $Da = 1.0$ (porous medium) at $\xi = 1.0$, the skin friction coefficient $(\mathrm{Re}_L^{1/2} C_f)$ increases approximately 104% as N increases from 1.0 to 5.0 while for the case without the porous medium ($Da \to \infty$), the skin friction coefficient $(\mathrm{Re}_L^{1/2} C_f)$ increases approximately 107% when N increases from $N = 1.0$ to 5.0.

In Figs. 3a and 3b, the angular velocity profile $\Omega(\xi, \eta)$ and wall stress coefficient (C_{fm}) for different values of the buoyancy ratio parameter (N) and the Darcy number (Da) are displayed, respectively. The negative values of the dimensionless angular velocity indicate that the micro rotation of sub-structures in the polar fluid is clock-wise. It is observed that the variation of N leads to decreases in the angular velocity. Further, the angular velocity is found to increase in the presence of the porous medium ($Da = 1.0$) as compared to the case without the porous medium ($Da \to \infty$). The wall stress coefficient (C_{fm}) increases with increasing values of N monotonously for increasing ξ values. In particular, at $\xi = 1.0$, the wall stress coefficient (C_{fm}) decreases approximately 60% as N decreases from 5.0 to 1.0 with the porous medium present ($Da = 1.0$) while in the absence of

Author's personal copy

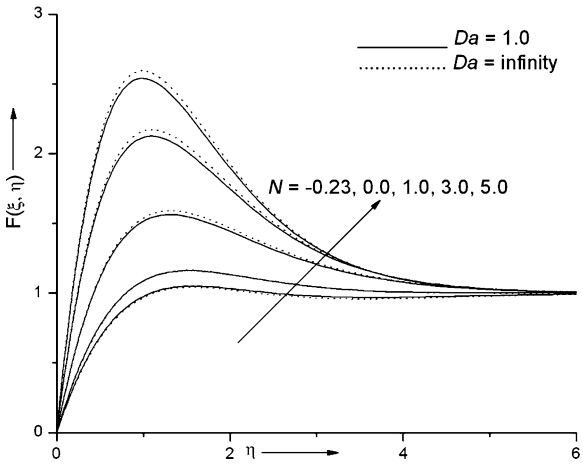

Fig. 2a Effects of N and Da on velocity profile for $\alpha = 1.0$, $\beta = 2.0$, $\lambda = 2.0$, $\Delta = 0.5$, $\xi = 1.0$, $\mathrm{Re}_L = 5.0$, $Sc = 0.22$, $Pr = 0.7$, $n = 1.0$, $Q = 0.5$ and $m = 0.5$

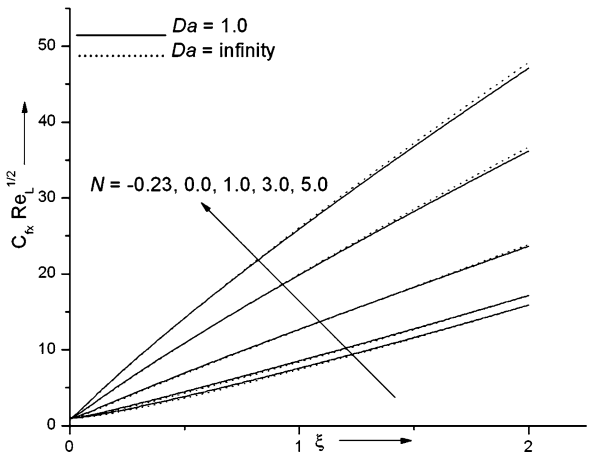

Fig. 2b Effects of N and Da on skin friction coefficient for $\alpha = 1.0$, $\beta = 2.0$, $\lambda = 2.0$, $\Delta = 0.5$, $\xi = 1.0$, $\mathrm{Re}_L = 5.0$, $Sc = 0.22$, $Pr = 0.7$, $n = 1.0$, $Q = 0.5$ and $m = 0.5$

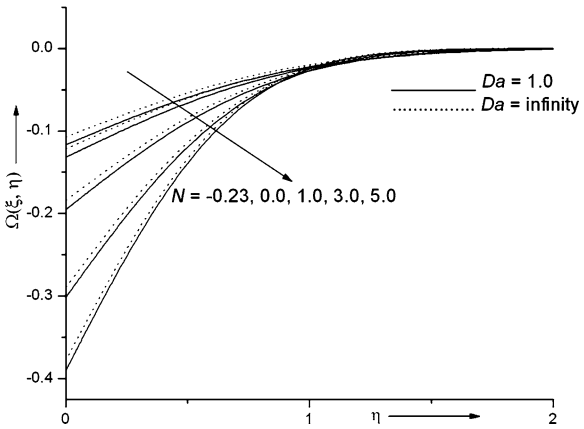

Fig. 3a Effects of N and Da on angular velocity profile for $\alpha = 1.0$, $\beta = 2.0$, $\lambda = 2.0$, $\Delta = 0.5$, $\xi = 1.0$, $\mathrm{Re}_L = 5.0$, $Sc = 0.22$, $Pr = 0.7$, $n = 1.0$, $Q = 0.5$ and $m = 0.5$

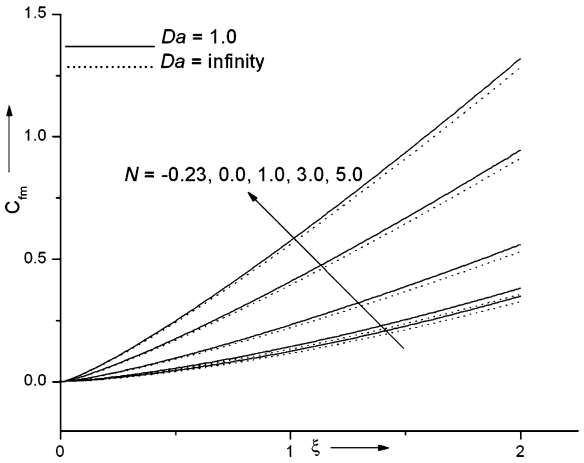

Fig. 3b Effects of N and Da on wall stress of angular velocity for $\alpha = 1.0$, $\beta = 2.0$, $\lambda = 2.0$, $\Delta = 0.5$, $\xi = 1.0$, $\mathrm{Re}_L = 5.0$, $Sc = 0.22$, $Pr = 0.7$, $n = 1.0$, $Q = 0.5$ and $m = 0.5$

the porous medium ($Da \to \infty$), the wall stress coefficient (C_{fm}) decreases approximately 61% when N decreases from $N = 5.0$ to 1.0.

The temperature profile $\Theta(\xi, \eta)$ and the wall heat transfer coefficient ($\mathrm{Re}_L^{-1/2} Nu_x$) are plotted in Figs. 4a and 4b, respectively, for different values of the buoyancy ratio parameter (N) and Darcy number (Da). The results indicate that an increase in the buoyancy ratio parameter (N) clearly induces a strong reduction in the temperature of the fluid and thus, resulting in a thinner thermal boundary layer. In addition, it is observed that the wall heat transfer coefficient ($\mathrm{Re}_L^{-1/2} Nu_x$) increases steadily with increasing values of ξ. For a fixed value of ξ, increasing the value of N has the tendency to decrease the fluid wall temperature as seen from Fig. 4a. This has the direct effect of increasing the wall heat transfer coefficient. It is also observed that with $N \leq 0$, the wall heat transfer coefficient ($\mathrm{Re}_L^{-1/2} Nu_x$) is found to reduce in the absence of the porous medium near the surface as compared to the case in which the porous medium is present. However, for the cases with $N > 0$, the wall heat transfer coefficient ($\mathrm{Re}_L^{-1/2} Nu_x$) is found to increase when the in porous medium away from the surface is present compared to the case in which the porous medium is absent. In particular, at $\xi = 1.0$, the value of ($\mathrm{Re}_L^{-1/2} Nu_x$) increases approxi-

Author's personal copy

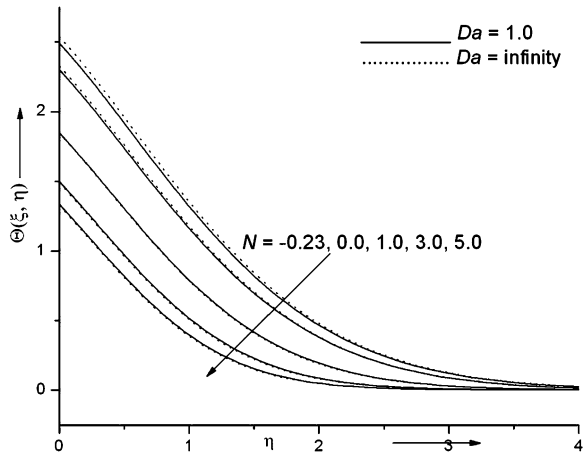

Fig. 4a Effects of N and Da on temperature profile for $\alpha = 1.0$, $\beta = 2.0$, $\lambda = 2.0$, $\Delta = 0.5$, $\xi = 1.0$, $\mathrm{Re}_L = 5.0$, $Sc = 0.22$, $Pr = 0.7$, $n = 1.0$, $Q = 0.5$ and $m = 0.5$

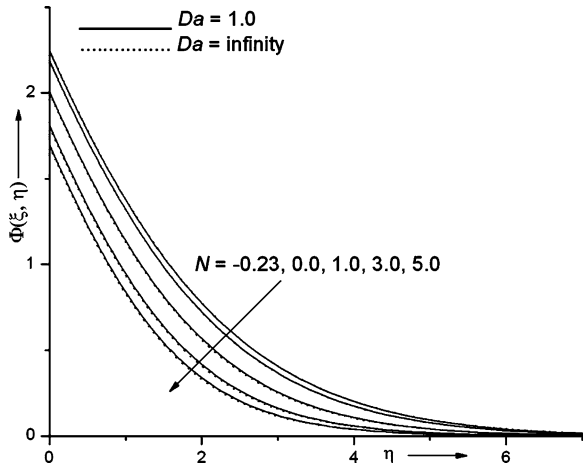

Fig. 5a Effects of N and Da on concentration profile for $\alpha = 1.0$, $\beta = 2.0$, $\lambda = 2.0$, $\Delta = 0.5$, $\xi = 1.0$, $\mathrm{Re}_L = 5.0$, $Sc = 0.22$, $Pr = 0.7$, $n = 1.0$, $Q = 0.5$ and $m = 0.5$

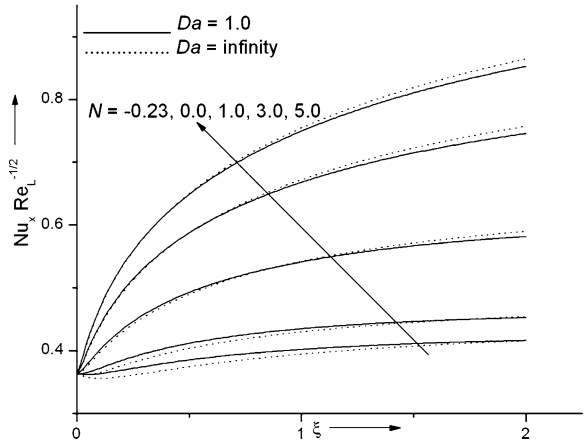

Fig. 4b Effects of N and Da on heat transfer coefficient for $\alpha = 1.0$, $\beta = 2.0$, $\lambda = 2.0$, $\Delta = 0.5$, $\xi = 1.0$, $\mathrm{Re}_L = 5.0$, $Sc = 0.22$, $Pr = 0.7$, $n = 1.0$, $Q = 0.5$ and $m = 0.5$

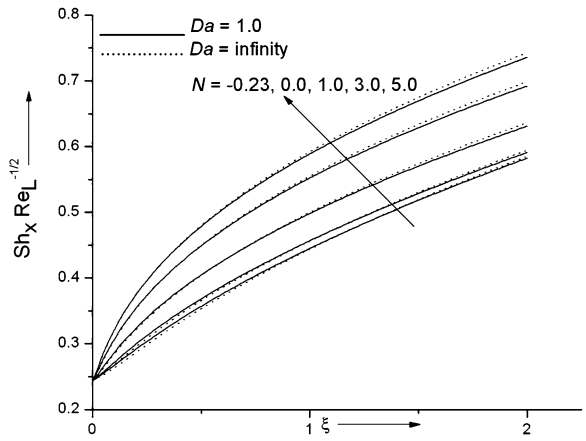

Fig. 5b Effects of N and Da on mass transfer coefficient for $\alpha = 1.0$, $\beta = 2.0$, $\lambda = 2.0$, $\Delta = 0.5$, $\xi = 1.0$, $\mathrm{Re}_L = 5.0$, $Sc = 0.22$, $Pr = 0.7$, $n = 1.0$, $Q = 0.5$ and $m = 0.5$

mately 38% as N increases from 1.0 to 5.0 in the presence of the porous medium ($Da = 1.0$) while when the porous medium is absent ($Da \to \infty$), the value of $(\mathrm{Re}_L^{-1/2} Nu_x)$ increases approximately 39% when N increases from $N = 1.0$ to 5.0.

In Figs. 5a and 5b, the concentration profile $\Phi(\xi, \eta)$ and the wall mass transfer coefficient $(\mathrm{Re}_L^{-1/2} Sh_x)$ for different values of the buoyancy of ratio parameter (N) and the Darcy number (Da) are depicted, respectively. It is seen that the concentration profile decreases with increasing values of N. The concentration profile does not show much change doe to the presence of the porous medium. The behavior of wall mass transfer coefficient $(\mathrm{Re}_L^{-1/2} Sh_x)$ is the same as in the case of the wall heat transfer coefficient $(\mathrm{Re}_L^{-1/2} Nu_x)$ discussed above. In particular, at $\xi = 1.0$, the value of $(\mathrm{Re}_L^{-1/2} Sh_x)$ increases approximately 18% as N increases from 1.0 to 5.0 in the presence of the porous medium ($Da = 1.0$) while in the absence of the porous medium ($Da \to \infty$), the value of $(\mathrm{Re}_L^{-1/2} Sh_x)$ increases approximately 19% when N increases from 1.0 to 5.0.

The velocity profile $F(\xi, \eta)$ and the skin friction coefficient $(\mathrm{Re}_L^{1/2} C_f)$ are presented in Figs. 6a and 6b, respectively, for different values of the buoyancy parameter (λ) and the fluid material parameter (α).

Author's personal copy

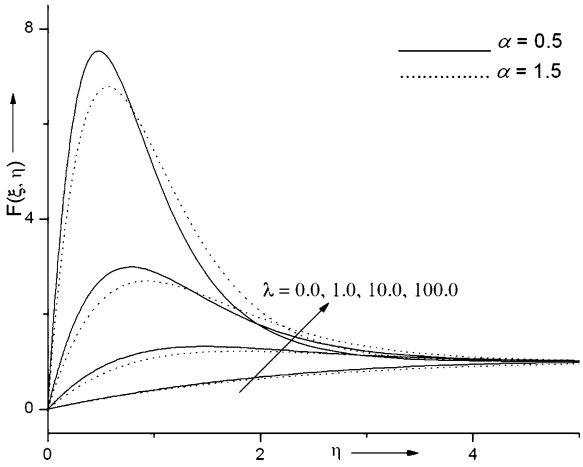

Fig. 6a Effects of λ and α on velocity profile for $N = 1.0$, $\beta = 2.0$. $Da = 1.0$, $\Delta = 0.5$, $\xi = 1.0$, $\mathrm{Re}_L = 5.0$, $Sc = 0.22$, $Pr = 0.7$, $n = 1.0$, $Q = 0.5$ and $m = 0.5$

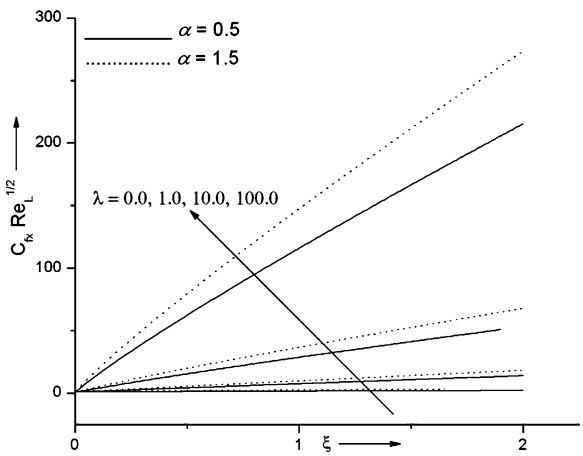

Fig. 6b Effects of λ and α on skin friction coefficient for $N = 1.0$, $\beta = 2.0$, $Da = 1.0$, $\Delta = 0.5$, $\xi = 1.0$, $\mathrm{Re}_L = 5.0$, $Sc = 0.22$, $Pr = 0.7$, $n = 1.0$, $Q = 0.5$ and $m = 0.5$

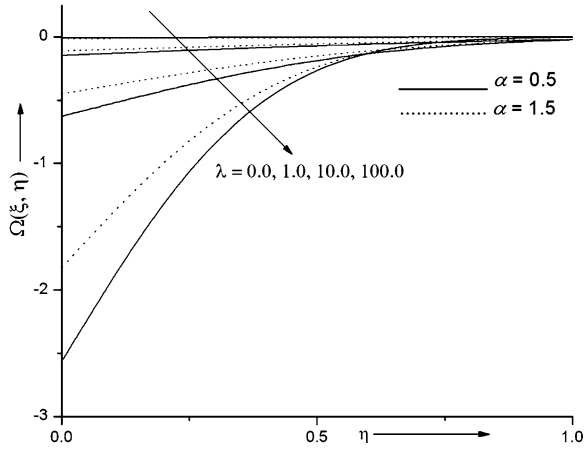

Fig. 7a Effects of λ and α on angular velocity profile for $N = 1.0$, $\beta = 2.0$, $Da = 1.0$, $\Delta = 0.5$, $\xi = 1.0$, $\mathrm{Re}_L = 5.0$, $Sc = 0.22$, $Pr = 0.7$, $n = 1.0$, $Q = 0.5$ and $m = 0.5$

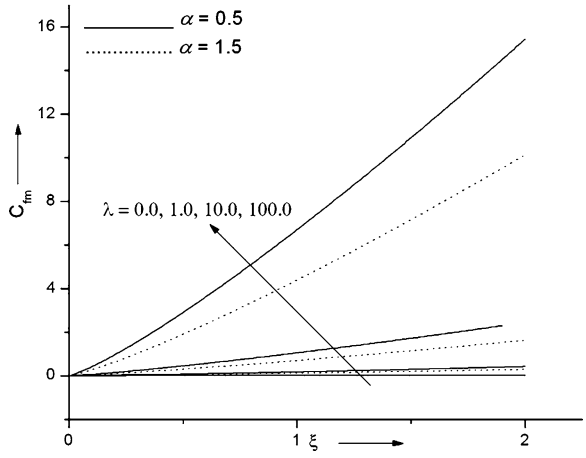

Fig. 7b Effects of λ and α on wall stress of angular velocity for $N = 1.0$, $\beta = 2.0$, $Da = 1.0$, $\Delta = 0.5$, $\xi = 1.0$, $\mathrm{Re}_L = 5.0$, $Sc = 0.22$, $Pr = 0.7$, $n = 1.0$, $Q = 0.5$ and $m = 0.5$

It is observed from Fig. 6a that, for buoyancy aiding flow ($\lambda > 0$), the buoyancy force shows significant overshoot in the velocity profile for both values of the material parameter α considered. The physical reason is that the combined effects of assisting buoyancy force due to thermal and concentration gradients and heat generation act like a favorable pressure gradient which enhances the fluid acceleration. Further, it is observed that the velocity decreases with increasing values of the material parameter α near the surface and increases as it goes away from the surface. The effects of the buoyancy parameter (λ) and the fluid material parameter (α) on the skin friction coefficient ($\mathrm{Re}_L^{1/2} C_f$) when $N = 1.0$, $n = 1.0$, $\beta = 2.0$, $Sc = 0.22$, $\Delta = 0.5$, $Pr = 0.7$, $\mathrm{Re}_L = 5.0$, $m = 0.5$, $Da = 1.0$ and $Q = 0.5$ are shown in Fig. 6a. It is observed that the skin friction coefficient ($\mathrm{Re}_L^{1/2} C_f$) increases with increasing values of the buoyancy parameter (λ) significantly. This is due to the fact that the increase of (λ) enhances the fluid acceleration and hence, the skin friction coefficient ($\mathrm{Re}_L^{1/2} C_f$) increases. In particular, for $\alpha = 0.5$ at $\xi = 1.0$, the skin friction coefficient ($\mathrm{Re}_L^{1/2} C_f$) increases approximately 287% as λ increases from 1.0 to 10.0 while for $\alpha = 1.5$ the skin friction coefficient ($\mathrm{Re}_L^{1/2} C_f$) increases approximately 277% when λ increases from $\lambda = 1.0$ to 10.0.

Author's personal copy

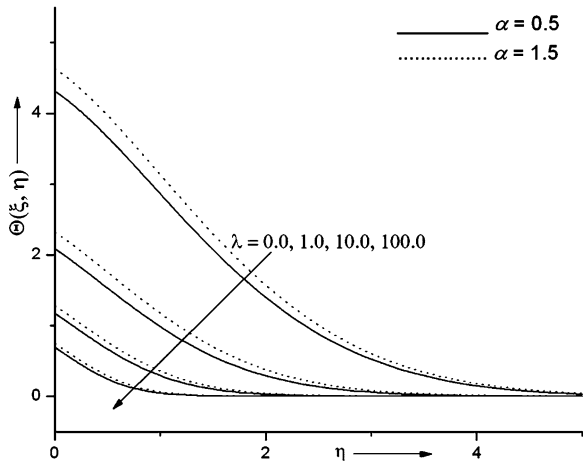

Fig. 8a Effects of λ and α on temperature profile for $N = 1.0$, $\beta = 2.0$, $Da = 1.0$, $\Delta = 0.5$, $\xi = 1.0$, $\mathrm{Re}_L = 5.0$, $Sc = 0.22$, $Pr = 0.7$, $n = 1.0$, $Q = 0.5$ and $m = 0.5$

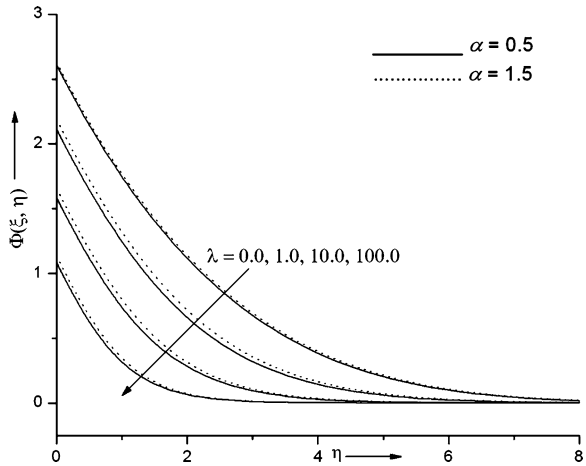

Fig. 9a Effects of λ and α on concentration profile for $N = 1.0$, $\beta = 2.0$, $Da = 1.0$, $\Delta = 0.5$, $\xi = 1.0$, $\mathrm{Re}_L = 5.0$, $Sc = 0.22$, $Pr = 0.7$, $n = 1.0$, $Q = 0.5$ and $m = 0.5$

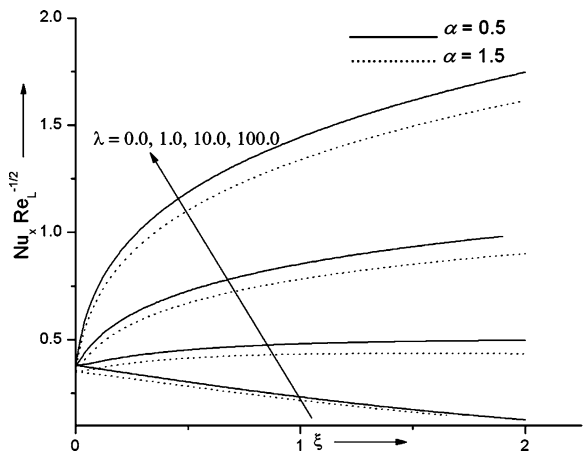

Fig. 8b Effects of λ and α on heat transfer coefficient for $N = 1.0$, $\beta = 2.0$, $Da = 1.0$, $\Delta = 0.5$, $\xi = 1.0$, $\mathrm{Re}_L = 5.0$, $Sc = 0.22$, $Pr = 0.7$, $n = 1.0$, $Q = 0.5$ and $m = 0.5$

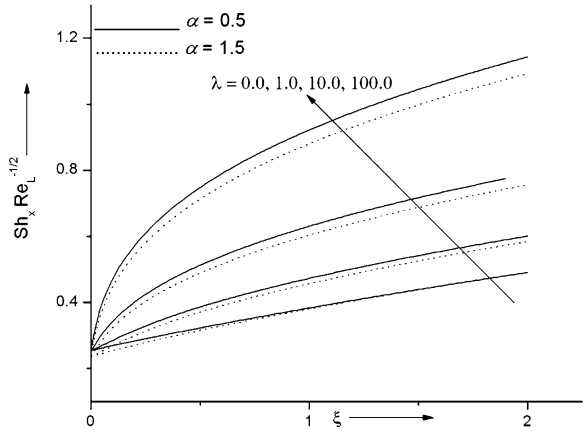

Fig. 9b Effects of λ and α on mass transfer rate for $N = 1.0$, $\beta = 2.0$, $Da = 1.0$, $\Delta = 0.5$, $\xi = 1.0$, $\mathrm{Re}_L = 5.0$, $Sc = 0.22$, $Pr = 0.7$, $n = 1.0$, $Q = 0.5$ and $m = 0.5$

The angular velocity profile $\Omega(\xi, \eta)$ and the wall stress coefficient (C_{fm}) are plotted in Figs. 7a and 7b, respectively, for different values of the buoyancy parameter (λ) and the fluid material parameter (α). It is noted that the variation of λ leads to a considerable decrease in the angular velocity. Further, the angular velocity is found to decrease with increasing values of the fluid material parameter (α). The wall stress coefficient (C_{fm}) increases with λ monotonously with increasing values of ξ. In particular, at $\xi = 1.0$, the value of (C_{fm}) decreases approximately 84% as λ decreases from 10.0 to 1.0 when $\alpha = 0.5$ while for $\alpha = 1.5$ the wall stress coefficient (C_{fm}) decreases approximately 83% when λ decreases from 10.0 to 1.0.

The effects of the buoyancy forces parameter (λ) and the fluid material parameter (α) on the temperature profile $\Theta(\xi, \eta)$ and the wall heat transfer coefficient ($\mathrm{Re}_L^{-1/2} Nu_x$) are shown in Figs. 8a and 8b, respectively. The results indicate that an increase in the fluid material parameter (α) clearly induces a strong increase in the temperature of the fluid and thus, results in a thicker thermal boundary layer. On the other hand, an increase in the buoyancy parameter (λ) induces a strong reduction in the fluid temperature and hence, results into a thinner thermal boundary layer. It

Author's personal copy

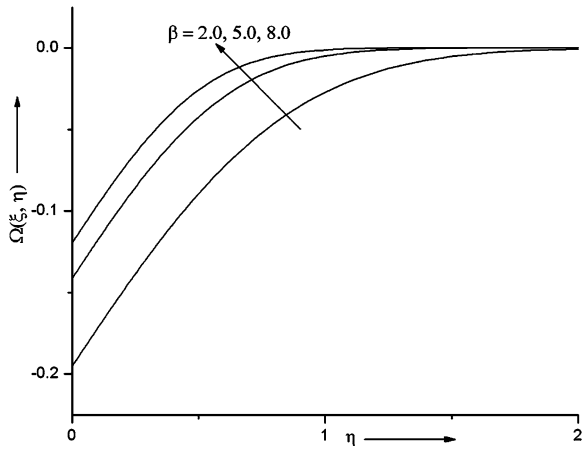

Fig. 10a Effects of β on angular velocity profile for $m = 0.5$, $N = 1.0$, $\lambda = 2.0$, $Da = 1.0$, $\Delta = 0.5$, $\xi = 1.0$, $\mathrm{Re}_L = 5.0$, $Sc = 0.22$, $Pr = 0.7$, $n = 1.0$, $Q = 0.5$ and $\alpha = 0.5$

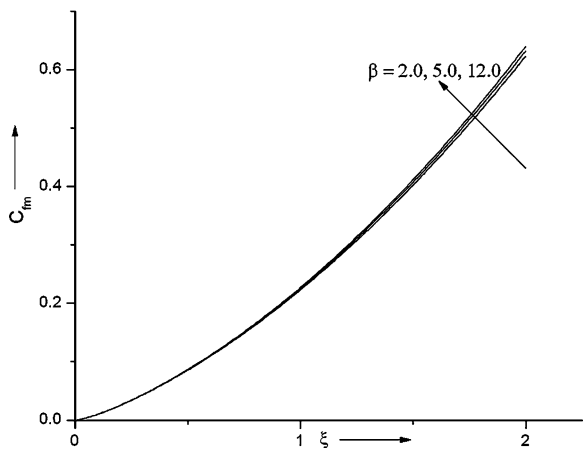

Fig. 10b Effects of β on wall stress of angular velocity for $N = 1.0$, $n = 1.0$, $Da = 1.0$, $Pr = 7.0$, $\xi = 1.0$, $\mathrm{Re}_L = 5.0$, $Sc = 2.57$, $\alpha = 2.0$, $Q = 0.5$, $\lambda = 5.0$, $\Delta = 0.5$ and $m = 0.5$

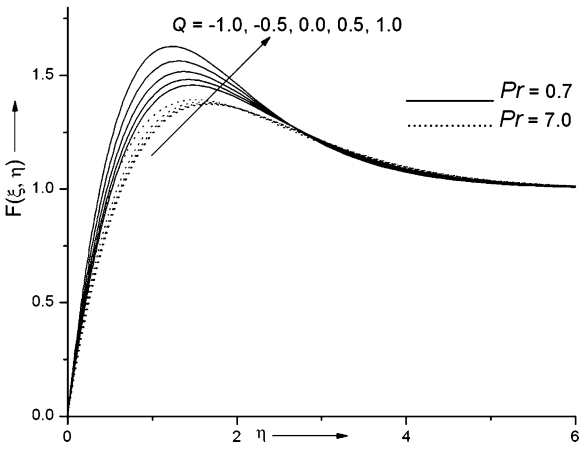

Fig. 11a Effects of Q and Pr on velocity profile for $N = 1.0$, $\beta = 2.0$, $Da = 1.0$, $\Delta = 0.5$, $\xi = 1.0$, $\mathrm{Re}_L = 5.0$, $Sc = 0.22$, $\alpha = 1.0$, $n = 1.0$, $\lambda = 2.0$ and $m = 0.5$

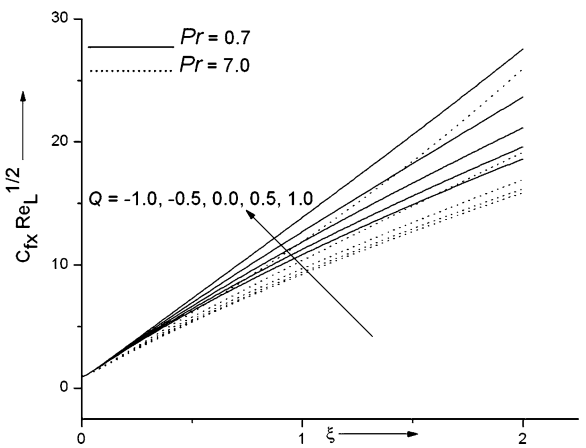

Fig. 11b Effects of Q and Pr on skin friction coefficient for $N = 1.0$, $\lambda = 2.0$, $Da = 1.0$, $\Delta = 0.5$, $\xi = 1.0$, $\mathrm{Re}_L = 5.0$, $Sc = 0.22$, $\beta = 2.0$, $m = 0.5$, $n = 1.0$ and $\alpha = 0.5$

is further observed that the wall heat transfer coefficient $(\mathrm{Re}_L^{-1/2} Nu_x)$ increases steadily with ξ and with increasing values of (λ) while it decreases with an increasing value of the fluid material parameter (α). In particular, at $\xi = 1.0$, the value of $(\mathrm{Re}_L^{-1/2} Nu_x)$ increases approximately 78% as (λ) increases from 1.0 to 10.0 for $\alpha = 0.5$ while for $\alpha = 1.5$, the value of $(\mathrm{Re}_L^{-1/2} Nu_x)$ increases approximately 81% when (λ) increases from 1.0 to 10.0.

Figures 9a and 9b illustrate the influence of the buoyancy parameter (λ) and the fluid material parameter (α) on the concentration profile $\Phi(\xi, \eta)$ and the wall mass transfer coefficient $(\mathrm{Re}_L^{-1/2} Sh_x)$, respectively. It is noted that an increase in the value of (λ) leads to a fall in the concentration profile while it enhances as the fluid material parameter (α) increases. It is further observed that the wall mass transfer coefficient $(\mathrm{Re}_L^{-1/2} Sh_x)$ increases monotonously with ξ and as (λ) increases while it decreases with an increasing value of the fluid material parameter (α). In particular, at $\xi = 1.0$, the value of $(\mathrm{Re}_L^{-1/2} Sh_x)$ increases approximately 46% as (λ) increases from 10.0 to 100.0 for $\alpha = 0.5$ while for $\alpha = 1.5$, the value of $(\mathrm{Re}_L^{-1/2} Sh_x)$ increases approximately 141% when (λ) increases from 10.0 to 100.0.

Author's personal copy

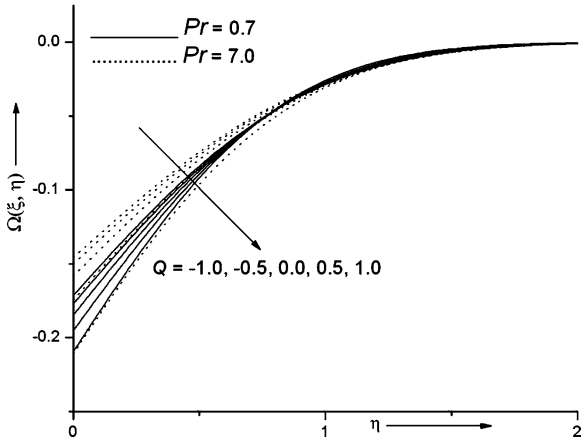

Fig. 12a Effects of Q and Pr on angular velocity profile for $N = 1.0$, $\beta = 2.0$, $Da = 1.0$, $\Delta = 0.5$, $\xi = 1.0$, $\mathrm{Re}_L = 5.0$, $Sc = 0.22$, $\alpha = 1.0$, $n = 1.0$, $\lambda = 2.0$ and $m = 0.5$

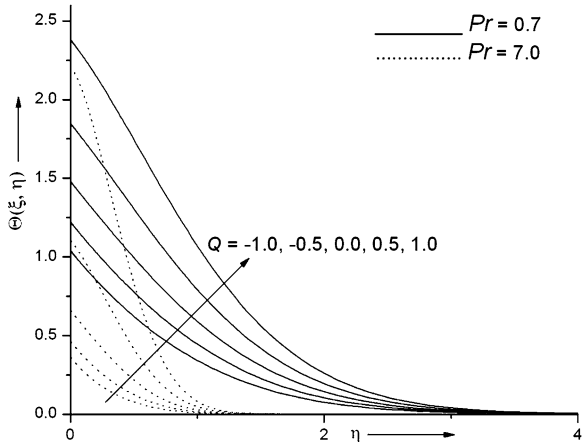

Fig. 13a Effects of Q and Pr on temperature profile for $N = 1.0$, $\beta = 2.0$, $Da = 1.0$, $\Delta = 0.5$, $\xi = 1.0$, $\mathrm{Re}_L = 5.0$, $Sc = 0.22$, $\alpha = 1.0$, $n = 1.0$, $\lambda = 2.0$ and $m = 0.5$

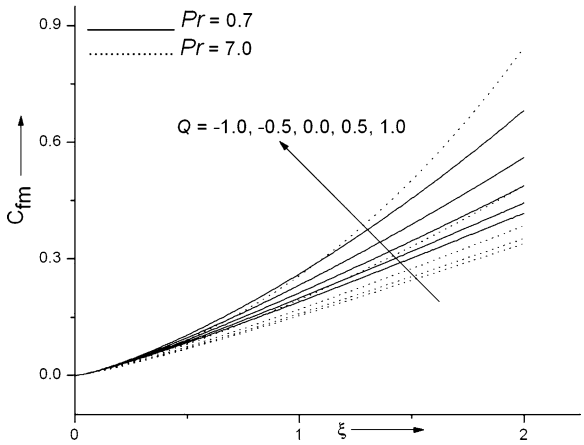

Fig. 12b Effects of Q and Pr on wall stress of angular velocity for $N = 1.0$, $\lambda = 2.0$, $Da = 1.0$, $\Delta = 0.5$, $\xi = 1.0$, $\mathrm{Re}_L = 5.0$, $Sc = 0.22$, $\beta = 2.0$, $m = 0.5$, $n = 1.0$ and $\alpha = 0.5$

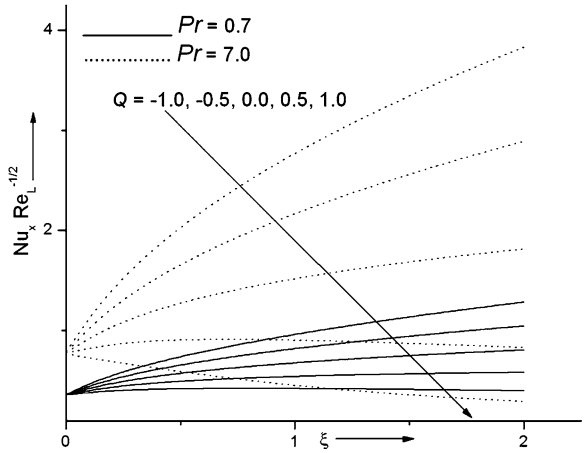

Fig. 13b Effects of Q and Pr on heat transfer rate for $N = 1.0$, $\lambda = 2.0$, $Da = 1.0$, $\Delta = 0.5$, $\xi = 1.0$, $\mathrm{Re}_L = 5.0$, $Sc = 0.22$, $\beta = 2.0$, $m = 0.5$, $n = 1.0$ and $\alpha = 0.5$

Figures 10a and 10b present the angular velocity profile $\Omega(\eta)$ and the wall stress coefficient (C_{fm}) for different values of the material parameter β, respectively. It is observed that the effects of the material parameter β on the dimensionless angular velocity are significant. An increase in the value of the material parameter β causes a rise in the dimensionless angular velocity which clearly indicates that the couple stresses are dominant during the rotation of the particles. The effects of the material parameter β on the wall stress coefficient (C_{fm}) when $\lambda = 2.0$, $n = 1.0$, $\beta = 2.0$, $Sc = 0.22$, $\Delta = 0.5$, $Pr = 0.7$, $\mathrm{Re}_L = 5.0$, $m = 0.5$, $\alpha = 1.0$ and $Q = 0.5$ are shown in Fig. 10b. It is clearly seen that the wall stress coefficient (C_{fm}) increases as β increases.

Figures 11a, 11b, 12a, 12b, 13a, 13b display the influence of the heat generation or absorption parameter Q and the Prandtl number Pr on the velocity $F(\xi, \eta)$, angular velocity $\Omega(\eta)$ and the temperature $\Theta(\xi, \eta)$ profiles, respectively, for $\lambda = 2.0$, $\mathrm{Re}_L = 5.0$, $Sc = 0.22$, $N = 1.0$, $n = 1.0$, $\Delta = 0.5$, $\xi = 1.0$, $Da = 1.0$, $\alpha = 1.0$, $\beta = 2.0$ and $m = 0.5$. It is noted that owing to the presence of a heat generation or a heat source effect $(Q > 0)$, the thermal state of the fluid increases. Hence, the temperature of the fluid increases within the boundary layer. In the

Author's personal copy

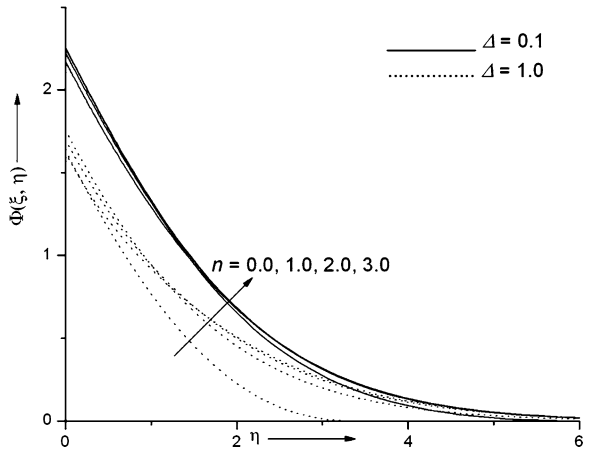

Fig. 14a Effects of n and Δ on concentration profile for $N = 1.0$, $\beta = 2.0$, $Da = 1.0$, $Pr = 0.7$, $\xi = 1.0$, $\mathrm{Re}_L = 5.0$, $Sc = 0.22$, $\alpha = 1.0$, $Q = 0.5$, $\lambda = 2.0$ and $m = 0.5$

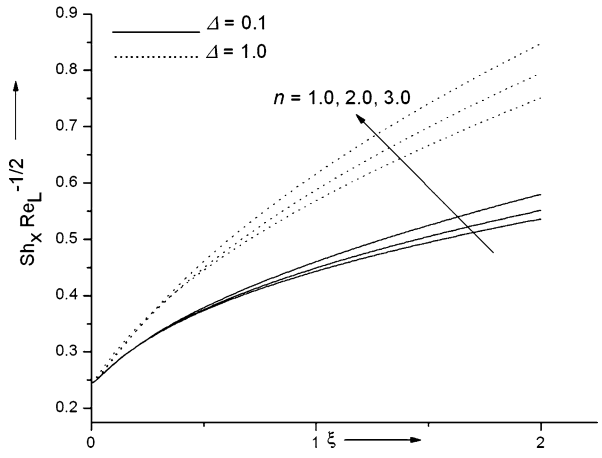

Fig. 14b Effects of n and Δ on mass transfer rate for $N = 1.0$, $\beta = 2.0$, $Da = 1.0$, $Pr = 0.7$, $\xi = 1.0$, $\mathrm{Re}_L = 5.0$, $Sc = 0.22$, $\alpha = 1.0$, $Q = 0.5$, $\lambda = 2.0$ and $m = 0.5$

event that the strength of the heat source is relatively large, an overshoot is observed in the temperature profiles within the thermal boundary layer as can be seen from Fig. 13a. Further, the effect of heat generation is more pronounced on the temperature profiles for high Prandtl number fluids ($Pr = 7.0$, water). Figure 11a displays that for $Pr = 7.0$, the velocity profile has approximately 8% overshoot with a thin velocity boundary layer. Conversely, the presence of a heat absorption or a heat sink effect ($Q < 0$) has the tendency to reduce the fluid temperature. This causes the thermal buoyancy effects to decrease resulting in a net reduction in the fluid velocity. These behaviors are clearly observed in Fig. 13a in which the magnitude of the temperature field decreases for ($Q < 0$). Moreover, it is also observed that the thickness of the thermal (temperature) boundary layer decreases as the heat absorption or heat sink effect increases. A similar behavior is obtained for the angular velocity profile which can be seen from Fig. 12a. The effects of the Prandtl number Pr and the heat generation or absorption parameter Q on the skin friction coefficient ($\mathrm{Re}_L^{1/2} C_f$) are shown in Fig. 11b. It is observed that an increase in the value of $|Q|$ leads to a rise in the skin friction coefficient ($\mathrm{Re}_L^{1/2} C_f$). In particular, for $Q = 0.5$ at $\xi = 1.0$, the skin friction coefficient ($\mathrm{Re}_L^{1/2} C_f$) decreases approximately 18% as Pr increases from 0.7 to 7.0, while for $Q = -0.5$ at $\xi = 1.0$, the skin friction coefficient ($\mathrm{Re}_L^{1/2} C_f$) decreases approximately 17% when the Prandtl number Pr increases from 0.7 to 7.0. The effect of Q and Pr on the wall heat transfer coefficient ($\mathrm{Re}_L^{-1/2} Nu_x$) is seen from Fig. 13b. In particular, for $Q = 0.5$ at $\xi = 1.0$, the wall heat transfer coefficient ($\mathrm{Re}_L^{-1/2} Nu_x$) increases approximately 67% as Pr increases from 0.7 to 7.0, while for $Q = -0.5$ at $\xi = 1.0$, the value of ($\mathrm{Re}_L^{-1/2} Nu_x$) increases approximately 165% when the Prandtl number Pr increases from 0.7 to 7.0. The physical reason is that the increase of Prandtl number from $Pr = 0.7$ (air) to $Pr = 7.0$ (water) indicates an enhancement in the viscosity of the fluid, which reduces the velocity within the boundary layer. As a result, the skin friction coefficient ($\mathrm{Re}_L^{1/2} C_f$) decreases. In contrast, an increase in the Prandtl number from $Pr = 0.7$ (air) to $Pr = 7.0$ (water) causes a corresponding reduction in the thermal conductivity of the fluid which is responsible for the increase in the heat transfer coefficient at the surface ($\mathrm{Re}_L^{-1/2} Nu_x$).

The effects of the chemical reaction parameter Δ and the order of the chemical reaction parameter n on the concentration profile $\Phi(\xi, \eta)$ and the wall mass transfer coefficient ($\mathrm{Re}_L^{-1/2} Sh_x$) when $\lambda = 2.0$, $\mathrm{Re}_L = 5.0$, $Sc = 0.22$, $N = 1.0$, $n = 1.0$, $\Delta = 0.5$, $\xi = 1.0$, $Da = 1.0$, $\alpha = 1.0$, $\beta = 2.0$ and $m = 0.5$ are presented in Figs. 14a and 14b, respectively. The values of the Schmidt number (Sc) are chosen to be more realistic, 0.22, 0.94, 2.57, representing diffusing chemical species of most common interest like water, propyl benzene hydrogen, water vapor and propyl benzene, etc., at 25 degree Celsius and one atmospheric pressure. The results indicate that as the order of the

Author's personal copy

chemical reaction parameter n increases, the concentration profile decreases at the surface whereas it increases away from the surface. Further, it is observed that the wall mass transfer coefficient ($\mathrm{Re}_L^{-1/2} Sh_x$) increases (the concentration between the wall and the fluid decreases) when the chemical reaction order n is increased. This is due to the fact that as n ($n = 1, 2, 3, \ldots$) increases, the power of Φ in the chemical reaction term increases. As the power of Φ increases, the effect of the chemical reaction as a source ($\Delta = 1.0$) gets strong. In particular, for $\Delta = 1.0$ at $\xi = 1.5$, the mass transfer coefficient ($\mathrm{Re}_L^{-1/2} Sh_x$) increases approximately 11% as the order of the chemical reaction parameter n increases from 1.0 to 3.0 while for $\Delta = 0.1$ at $\xi = 1.5$, the wall mass transfer coefficient ($\mathrm{Re}_L^{-1/2} Sh_x$) increases approximately 6% when the order of the chemical reaction parameter n increases from 1.0 to 3.0.

5 Conclusions

A detailed numerical study has been carried out for mixed convection flow of a polar fluid through a porous medium over a vertical plate in the presence of internal heat generation or absorption and homogeneous n^{th} order chemical reaction. The final set of non-similar, coupled nonlinear, partial differential equations is solved using an implicit finite difference scheme in combination with quasi-linearization technique. The main conclusions of this study are summarized as follows:

1. The buoyancy parameter λ and the ratio of the buoyancy forces N are found to cause overshoot in the velocity profile.
2. The effects of the material parameters α and β are found to be significant on the velocity, angular velocity, temperature and concentration profiles.
3. A relatively high Prandtl number $Pr = 7.0$ (water) causes a thinner thermal boundary layer in the presence of heat generation or absorption ($Q > 0$ or $Q < 0$).The heat generation effect ($Q > 0$) causes a thicker velocity and thermal boundary layers while a heat absorption effect ($Q < 0$) has the tendency to reduce the thickness of the velocity and thermal boundary layers.
4. The velocity decreases in the presence of a porous medium as compared to the case when the porous medium is absent.
5. The effects of the chemical reaction parameter Δ and the order of chemical reaction parameter n are found to be significant on the wall mass transfer coefficient.
6. The order of the chemical reaction parameter n is found to cause a thinner concentration boundary layer.

Acknowledgements Authors are thankful to the anonymous Reviewers for their useful detailed comments. Dr. P.M. Patil wishes to express his sincere thanks to University Grants Commission, South Western Regional Office, Bangalore, India, for the financial support under the Minor Research Project No. MRP(S)-636/09-10/KAKA060/UGC-SWRO. Also, Dr. Patil dedicates this paper to Shri Rakesh Singh, IAS, Officer on Special Duty to the Ministry of Law and Justice, Government of India for his outstanding service to the people of India.

Nomenclature

C	species concentration
C_a, C_d	coefficients of couple stress viscosities
C_{fm}	wall stress of angular velocity
C_{fx}	local skin friction coefficient
C_p	specific heat at constant pressure
C_∞	species concentration far away from the wall
D	mass diffusivity
Da	Darcy number
F	dimensionless velocity component
f	dimensionless stream function
g	acceleration due to gravity
Gr, Gr^*	Grashof numbers due to temperature and concentration, respectively
I	a constant of same dimension as that of the moment of inertia of unit mass
k	thermal conductivity of the fluid
k_1	first order chemical reaction rate
K	permeability of the porous medium
L	characteristic length
n	exponent of chemical reaction
N	ratio of the buoyancy forces (Grashof numbers)
m_w	mass flux per unit area at the plate
Nu_x	local Nusselt number
Pr	Prandtl number
q_w	heat flux per unit area at the plate
Q_0	heat generation coefficient
Q	heat generation or absorption parameter
Re_L	Reynolds number

Author's personal copy

Sc	Schmidt number
Sh_x	local Sherwood number
T	temperature in the boundary layer
T_∞	temperature of fluid far away from the wall
u, v	components of velocities along and perpendicular to the plate, respectively
x, y	coordinate system

Greek symbols

α, β	material parameters characterizing the polarity of the fluid
β_T, β_C	volumetric coefficients of the thermal and concentration expansions, respectively
γ	spin gradient
ψ	stream function
Δ	chemical reaction parameter
λ, λ^*	buoyancy parameters due to temperature and concentration gradients, respectively
ξ, η	transformed variables
Θ, Φ	dimensionless temperature and concentration, respectively
ω	angular velocity of rotation of particles
ρ	density of the fluid
μ	dynamic viscosity of the fluid
ν	kinematic viscosity
ν_r	rotational kinematic viscosity
Ω	dimensionless angular velocity

Subscripts

C	of concentration
T	of temperature
w, ∞	conditions at the wall and infinity, respectively
ξ, η	denote the partial derivatives w.r.t. these variables, respectively

References

1. Nield DA, Bejan A (2006) Convection in porous media, 3rd edn. Springer, New York
2. Ingham DB, Pop I (eds) (2005) Transport phenomena in porous media. Elsevier, Oxford
3. Vafai K (ed) (2005) Handbook of porous media, 2nd edn. Taylor & Francis, New York
4. Ingham DB, Bejan A, Mamut E, Pop I (eds) (2004) Emerging technologies and techniques in porous media. Kluwer, Dordrecht
5. Bejan A, Dincer I, Lorente S, Miguel AF, Reis AH (2004) Porous and complex flow structures in modern technologies. Springer, New York
6. Merkin JH (1980) Mixed convection boundary layer flow on a vertical surface in a saturated porous medium. J Eng Math 14:301–303
7. Merkin JH (1985) On dual solutions occurring in mixed convection in a porous medium. J Eng Math 20:171–179
8. Aly EH, Elliot L, Ingham DB (2003) Mixed convection boundary layer flow over a vertical surface embedded in a porous medium. Eur J Mech B, Fluids 22:529–543
9. Nazar R, Pop I (2004) Mixed convection boundary layer flow over a vertical surface in a porous medium with variable surface heat flux. In: Recent advances and applications in heat and mass transfer. IMECE, Kuwait, pp 87–97
10. Chin KE, Nazar R, Arifin NM, Pop I (2007) Effect of variable viscosity on mixed convection boundary layer flow over a vertical surface embedded in a porous medium. Int Commun Heat Mass Transf 34:464–473
11. Das UN, Deka RK, Soundalgekar VM (1994) Effects of mass transfer on the flow past an impulsively started infinite vertical plate with constant heat flux and chemical reaction. Forsch Ingenieurwes 60:284–287
12. Muthucumaraswamy R, Ganesan P (2000) On impulsive motion of a vertical plate with heat flux and diffusion of chemically reactive species. Forsch Ingenieurwes 66:17–23
13. Muthucumaraswamy R, Ganesan P (2001) First order chemical reaction on flow past an impulsively started vertical plate with uniform heat and mass flux. Acta Mech 147:45–57
14. Seddeek MA (2005) Finite element method for the effects of chemical reaction, variable viscosity, thermophoresis and heat generation/absorption on a boundary layer hydromagnetic flow with heat and mass transfer over a heat surface. Acta Mech 177:1–18
15. Kandasamy R, Perisamy K, Sivagnana Prabhu KK (2005) Effects of chemical reaction, heat and mass transfer along a wedge with heat source and concentration in the presence of suction or injection. Int J Heat Mass Transf 48:1388–1394
16. Kandasamy R, Perisamy K, Sivagnana Prabhu KK (2005) Chemical reaction, heat and mass transfer on MHD flow over a vertical stretching surface with heat source and thermal stratification effects. Int J Heat Mass Transf 48:4557–4561
17. Raptis A, Perdikis C (2006) Viscous flow over a nonlinearly stretching sheet in the presence of a chemical reaction and magnetic field. Int J Non-Linear Mech 42:527–529
18. Jalaal M, Ganji DD, Ahmadi G (2010) Analytical investigation on acceleration motion of a vertically falling spherical particle in incompressible Newtonian media. Adv Powder Technol 21(3):298–304
19. Jalaal M, Ganji DD (2010) On unsteady rolling motion of spheres in inclined tubes filled with incompressible Newtonian fluids. Adv Powder Technol. doi:10.1016/j.apt.2010.03.011
20. Jalaal M, Ganji DD (2010) An analytical study on motion of a sphere rolling down an inclined plane submerged in a Newtonian fluid. Powder Technol 198(1):82–92
21. Jalaal M, Ganji DD, Ahmadi G (2010) An analytical study on settling of non-spherical particles. Asia-pacific J Chem Eng. doi:10.1002/apj.492

Author's personal copy

22. Cowin SC (1974) The Theory of polar fluids. Adv Appl Mech 14:279
23. Patil PM, Hiremath PS (1992) A note on the effect of couple stresses on the flow through a porous medium. Rheol Acta 21:206–207
24. Hiremath PS, Patil PM (1993) Free convection effects on the oscillatory flow of a couple stress fluid through a porous medium. Acta Mech 98:143–158
25. Raptis A, Takhar HS (1999) Polar fluid through a porous medium. Acta Mech 135:91–93
26. Ogulu A (2005) On the oscillating plate temperature flow of a polar fluid past a vertical porous plate in the presence of couple stresses and radiation. Int Commun Heat Mass Transf 32:1231–1243
27. Patil PM, Kulkarni PS (2008) Effects of chemical reaction on free convective flow of a polar fluid through a porous medium in the presence of internal heat generation. Int J Therm Sci 47:1043–1054
28. Gorla RSR (1992) Mixed convection in a micropolar fluid from a vertical surface with uniform heat flux. Int J Eng Sci 30:349–358
29. Patil PM (2008) Effects of free convection on the oscillatory flow of a polar fluid through a porous medium in presence of variable wall heat flux. J Eng Phys Thermophys 81(5):905–922
30. Patil PM, Kulkarni PS (2009) Free convective oscillatory flow of a polar fluid through a porous medium in the presence of oscillating suction and temperature. J Eng Phys Thermophys 82(6):1138–1145
31. Inouye K, Tate A (1974) Finite difference version quasilinearisation applied to boundary layer equations. AIAA J 12:558–560
32. Singh PJ, Roy S, Pop I (2008) Unsteady mixed convection from a rotating vertical slender cylinder in an axial flow. Int J Heat Mass Transf 51:1423–1430
33. Schlichting H (2000) Boundary layer theory. Springer, New York
34. Varga RS (2000) Matrix iterative analysis. Prentice Hall, New York
35. Elbashbeshy EMA, Bazid MA (2002) The mixed convection along a vertical plate with variable surface flux embedded in porous medium. Appl Math Comput 125:317–324